Front. Phys. 12(5), 128703 (2017)
DOI 10.1007/s11467-017-0688-4

RESEARCH ARTICLE

Mesoscopic model for binary fluids

C. Echeverria[1], K. Tucci[1,2], O. Alvarez-Llamoza[3,4], E. E. Orozco-Guillén[5], M. Morales[6], M. G. Cosenza[2,†]

[1] *CeSiMo, Universidad de Los Andes, Mérida 5251, Mérida, Venezuela*
[2] *Grupo de Caos y Sistemas Complejos, Centro de Física Fundamental, Universidad de Los Andes, Mérida, Venezuela*
[3] *Departamento de Física, FACYT, Universidad de Carabobo, Valencia, Venezuela*
[4] *Facultad de Ingeniería, Universidad Católica de Cuenca, Ecuador*
[5] *Programa Académico de Ingeniería en Energía, Universidad Politécnica de Sinaloa, 82199 Mazatlán, Mexico*
[6] *Programa Académico de Ingeniería en Nanotecnología, Universidad Politécnica de Sinaloa, 82199 Mazatlán, Mexico*
Corresponding author. E-mail: [†] *mario.cosenza@gmail.com*
Received November 17, 2016; accepted March 22, 2017

We propose a model for studying binary fluids based on the mesoscopic molecular simulation technique known as multiparticle collision, where the space and state variables are continuous, and time is discrete. We include a repulsion rule to simulate segregation processes that does not require calculation of the interaction forces between particles, so binary fluids can be described on a mesoscopic scale. The model is conceptually simple and computationally efficient; it maintains Galilean invariance and conserves the mass and energy in the system at the micro- and macro-scale, whereas momentum is conserved globally. For a wide range of temperatures and densities, the model yields results in good agreement with the known properties of binary fluids, such as the density profile, interface width, phase separation, and phase growth. We also apply the model to the study of binary fluids in crowded environments with consistent results.

Keywords multiparticle collision dynamics, mesoscopic models, phase separation, interface dynamics

PACS numbers 89.75.Fb, 05.50.+q, 87.23.Ge

1 Introduction

In recent years, there has been much interest in the development of computational models for simulation of fluid dynamics on the basis of particle interactions [1–4]. In many fluid simulation problems, the potential energy of a moderate number of particles is sufficient to represent some macroscopic behaviors. However, to study phenomena such as the mobility of colloids, chemical reactions of macromolecules, fluid diffusion in crowded media, or the dynamics of phase segregation, a large number of particles is required to obtain good descriptions. For such problems, several mesoscopic simulation techniques have been implemented, for example, lattice gas automata [5], lattice Boltzmann methods for fluid dynamics [6] and for multiphase flows [7–9], dissipative particle dynamics [10, 11], smoothed particle dynamics [12], and multiparticle collision dynamics [13–15]. Each of these techniques provides a coarse-grained approach that incorporates conservation laws and the essential physics while omitting corpuscular details.

Multiparticle collision dynamics, also known as stochastic rotation dynamics [16], is a particle-based technique for complex fluids that includes thermal fluctuations and hydrodynamic interactions [13]. Multiparticle collision dynamics has proven to be capable of simulating many soft-matter systems, including colloids [14, 17, 18], polymers and proteins [19–24], vesicles [25], and reactive systems [26, 27]. Multiparticle collision dynamics has also been employed to investigate the properties of chemical reactions in crowded environments, i.e., media containing obstacles [28–30].

In particular, owing to their spatial and temporal scales, binary fluid systems are well suited for simulation through multiparticle collision techniques. There are two main approaches for simulating a binary fluid in the context of multiparticle collision dynamics. The first, proposed by Hashimoto *et al.* [31], incorporates an additional collision step in the multiparticle collision scheme to guide the mean particle flow of each species in the

*arXiv: 1606.06401.

direction of its density gradient. These authors studied segregation phenomena in a binary fluid and observed the formation of drop-shaped domains with curvatures that can be described by Laplace's law. An extension of this approach has been used to describe amphiphilic fluids [32] and compounds consisting of hydrophilic and hydrophobic parts [33]. Although this extension of the multiparticle collision technique conserves energy and momentum, it has not been proven to yield thermodynamically consistent results [34].

The second approach extends multiparticle collision dynamics to a binary mixture where particles of different species collide in supercells, while the rest of the multiparticle collision process occurs in smaller cells [35]. This approach can simulate phase separation phenomena, although it requires the use of a shifting technique to ensure Galilean invariance [36]. However, phase separation is achieved at very low temperatures, at which strong correlations usually appear among particles.

In this article, we propose a multiparticle collision model with a repulsion rule to investigate phase separation processes in a binary fluid in both free and crowded environments. In Section 2, we present the model and introduce the repulsion rule for the collision dynamics between the centers of mass of particles of different species. We show that this rule preserves the mass and energy of the system and discuss the conservation of momentum and Galilean invariance. In Section 3, the model is employed to study the behavior of a binary fluid in a free environment. We investigate several phenomena in a wide range of temperatures, including the stability of an interface front between the two species, phase separation and phase growth, and calculate the characteristic parameters for these processes. The simulation results are shown to be in good agreement with theoretical models. In Section 4, we simulate the properties of a binary fluid in a crowded environment by considering particles of both species moving through a random distribution of stationary obstacles. Under this condition, we describe the stabilization of the interface and the formation of domains. Conclusions are presented in Section 5.

2 Segregation rules in multiparticle collision dynamics

Multiparticle collision models simplify the dynamical description while retaining the essential features of molecular dynamics [13–15]. We consider a fluid consisting of particles of two species, A and B. The masses of particles of species A and B are m^A and m^B, respectively. Particles of both species, with continuous positions and velocities, stream freely between multiparticle collision events that occur at discrete time intervals τ. To obtain collisions, the volume $\mathcal{V}$ of the system is divided into cubic cells with length $\ell = 1$ labeled by an index ξ. We denote by n_ξ^γ the number of particles of species γ in cell ξ, where γ can take the value A or B. The center-of-mass velocity of particles of species γ in cell ξ before collision is given by

$$\boldsymbol{V}_\xi^\gamma = \frac{1}{n_\xi^\gamma}\sum_{i=1}^{n_\xi^\gamma} \boldsymbol{v}(i)_\xi^\gamma, \tag{1}$$

where $\boldsymbol{v}(i)_\xi^\gamma$ is the pre-collision velocity of particle i of species γ in cell ξ.

Segregation in binary fluids can be simulated by including repulsion effects among species similar to those employed in models of spinodal decomposition with molecular dynamics [37]. Thus, we define the center-of-mass velocity of particles of species γ after all-species collisions as

$$\widetilde{\boldsymbol{V}}_\xi^\gamma = \frac{\kappa\rho_\xi^{\gamma^*} m_{\gamma^*}\widehat{\boldsymbol{r}}_{\gamma\gamma^*} + \boldsymbol{V}_\xi^\gamma}{|\kappa\rho_\xi^{\gamma^*} m_{\gamma^*}\widehat{\boldsymbol{r}}_{\gamma\gamma^*} + \boldsymbol{V}_\xi^\gamma|}|\boldsymbol{V}_\xi^\gamma|, \tag{2}$$

where γ^* represents a species other than γ, $\rho_\xi^{\gamma^*}$ is the density of particles of species γ^* in cell ξ, $\widehat{\boldsymbol{r}}_{\gamma\gamma^*}$ is the unit vector in the direction between the centers of mass of species γ and γ^*, $|\cdots|$ is the vector norm, and κ is a parameter representing the repulsive force between different species. Note that if $\rho_\xi^{\gamma^*} = 0$, i.e., if there are no particles of species γ^* in cell ξ, then the center-of-mass velocity of particles of species γ does not change; i.e., $\widetilde{\boldsymbol{V}}_\xi^\gamma = \boldsymbol{V}_\xi^\gamma$. We calculate the velocity of particles of species γ with respect to the velocity of the center of mass after the collision as

$$\widetilde{\boldsymbol{v}}(i)_\xi^\gamma = \widetilde{\boldsymbol{V}}_\xi^\gamma + (\boldsymbol{v}(i)_\xi^\gamma - \boldsymbol{V}_\xi^\gamma). \tag{3}$$

Next, we apply the one-species rotation defined as

$$\boldsymbol{v}'(i)_\xi^\gamma = \sum_\gamma \left(\widetilde{\boldsymbol{V}}_\xi^\gamma + \widehat{\omega}_\xi^\gamma(\widetilde{\boldsymbol{v}}(i)_\xi^\gamma - \widetilde{\boldsymbol{V}}_\xi^\gamma)\right), \tag{4}$$

where $\widehat{\omega}_\xi^\gamma$ is a randomly chosen rotation operator applied only to particles of species γ.

The rule introduced in Eq. (2) can also be seen as a rotation of the velocity vector of the center of mass of each species in the opposite direction to the center of mass of the other species. Note that the multiparticle collision model with repulsion conserves both energy and mass in each cell ξ after each multiparticle collision event. Linear momentum is conserved within a homogeneous phase, but not at the interfaces. We verified the Galilean invariance of the simulations by checking that the diffusion coefficient of the system is independent of the spatial direction [36].

3 Binary fluid in a free environment

3.1 Diffusion coefficient

Phase separation and the formation of stable interfaces in binary fluids usually occur at low temperatures. To study the behavior of the multiparticle-collision repulsion model at low temperatures, we first consider the case of a single species. Then, only rules (1) and (4) apply, with $\widetilde{\boldsymbol{V}}_\xi^\gamma = \boldsymbol{V}_\xi^\gamma$. The volume is defined as $\mathcal{V} = L_x \times L_y \times L_z = 50^3$, with periodic boundary conditions. In each simulation step $\tau = 1$, the rotation operators $\widehat{\omega}_\xi$ are taken to describe rotation angles $\theta = \pm\pi/2$ about randomly chosen axes. The number of particles in the system is $N = \mathcal{V}\rho$, where ρ is the mean density of particles.

Assuming that collision events are not correlated, it has been shown that the diffusion coefficient for a single species in multiparticle collision dynamics can be approximated by the expression [27]

$$D = \frac{k_B T \tau}{2m}\left[\frac{3\rho}{\rho - 1 + \mathrm{e}^{-\rho}(1-\cos\theta)} - 1\right], \tag{5}$$

where k_B is the Boltzmann constant, and the temperature T is given in reduced units. This equation is satisfied when the average displacement of the particles between collisions is of the order of the size of the cell, i.e., when $T \approx 1$.

Figure 1 shows the diffusion coefficient D for a single species as a function of the density, calculated from the simulations and compared with Eq. (5), for different temperatures.

Note that at low temperatures, the diffusion coefficient calculated from the simulations agrees with the mesoscopic diffusion coefficient given by Eq. (5). These results show that multiparticle collision models can be used to simulate systems with relatively low temperatures ($T = 0.06$) while maintaining good diffusive behavior.

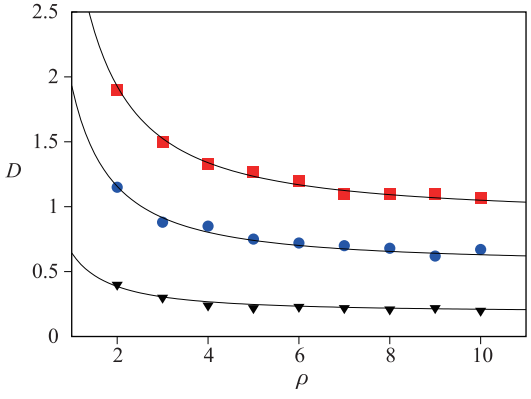

Fig. 1 Diffusion coefficient D as a function of the density of particles ρ for a single species, calculated from simulation of the model for three temperatures: $T = 0.3$ (*squares*), $T = 0.18$ (*circles*), and $T = 0.06$ (*triangles*). Solid lines correspond to Eq. (5).

3.2 Interface stability

To implement the multiparticle collision model with repulsion, Eqs. (1)–(4), we consider a three-dimensional film with length $L_x = 100$ units along x, width $L_y = 100$ units along y, and height $L_z = 2$ units along z. We impose periodic boundary conditions in the y and z directions, and bounce-back reflection boundary conditions on both the left and right sides of the film along the x direction. The average number of particles per cell is assumed to be the same for both species; i.e., $n^A = n^B \equiv n$. Additionally, we assume species with equal masses; i.e., $m^A = m^B \equiv m$.

First, we study the properties of the interface between the two fluids. As an initial condition, particles of species A are uniformly distributed at random on the right side of the film so that their mean density, averaged over cells, is $\rho^A(x \geq 50) = 2mn$ and $\rho^A(x < 50) = 0$, and particles of species B are similarly distributed on the left side of the film; i.e., $\rho^B(x \leq 50) = 2mn$, and $\rho^B(x > 50) = 0$.

Figure 2(a) shows a snapshot of the initial condition of the system. Figures 2(b) and (c) show snapshots of the system at $t = 10^5$ iterations with parameters $n = 5$ and $n = 8$, respectively. Note that in both Fig. 2(b) and Fig. 2(c), the system maintains two phases separated by a thin region where species A and B are mixed. That is, the multiparticle-collision repulsion model can yield a stable interface for some values of the system parameters.

To characterize the interface, we calculate the normalized density profile, which is defined as

$$\Delta\rho^\gamma(x) = \frac{\rho^\gamma(x) - \rho^{\gamma^*}(x)}{\rho^\gamma_\infty}, \tag{6}$$

where $\rho^\gamma(x)$ is the mean density of species γ in cells with

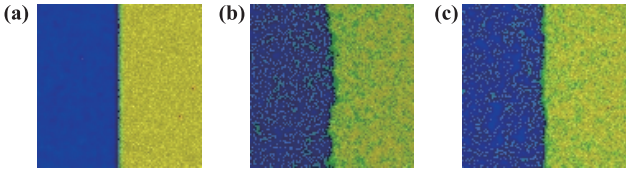

Fig. 2 Snapshots along the z axis of the system for $T = 0.12$ and $\kappa = 5$. Particles of species A appear in yellow (*light gray*), and particles of species B are marked in blue (*black*). Green (*dark gray*) indicates the presence of particles of both species. The color intensity is proportional to the particle density. **(a)** Initial state. **(b)** State after $t = 10^5$ iterations for $n = 5$. **(c)** State after $t = 10^5$ iterations for $n = 8$.

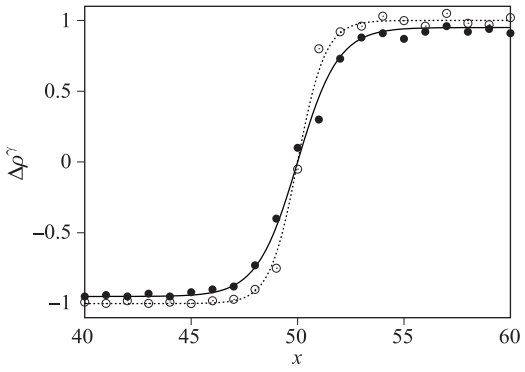

Fig. 3 Variation of the normalized profile density $\Delta\rho^\gamma(x)$ as a function of x for $n = 5$ (*solid circles*) and $n = 8$ (*open circles*), with fixed parameter values $T = 0.12$, $\kappa = 5.0$. Solid and dashed lines are fittings of Eq. (7) for $n = 5$ and $n = 8$, respectively.

coordinate x, and $\rho^\gamma_\infty = 2mn$ is the value of $\rho^\gamma(x)$ far from the interface.

Figure 3 shows the variation of the normalized density profile for two different numbers of particles per cell. Note that as the number of particles per cell increases, the interface becomes sharper. This effect is expected because the repulsion between particles of different species increases as their densities increase.

To measure the interface width, denoted by ζ,we fitted the simulation points in the interface profile of Fig. 3 with the function [38]

$$\Delta\rho^\gamma(x) = \tanh\left(\frac{x}{\zeta}\right). \tag{7}$$

The behavior of the interface width ζ as a function of the repulsion parameter κ is shown in Fig. 4. There is a critical value, $\kappa_c \approx 0.6$, above which ζ reaches an asymptotic

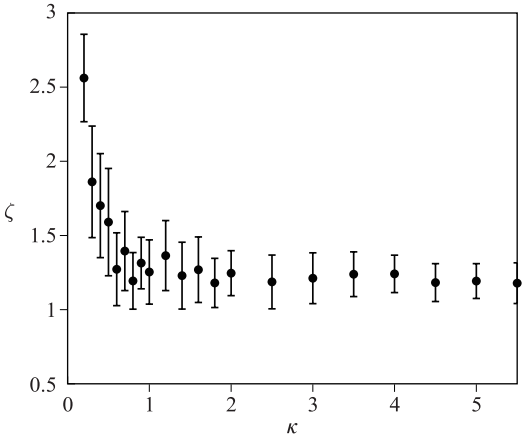

Fig. 4 Mean interface width ζ as a function of the repulsion parameter κ with fixed parameter values $n = 5$ and $T = 0.12$ after $t = 10^5$ iterations.

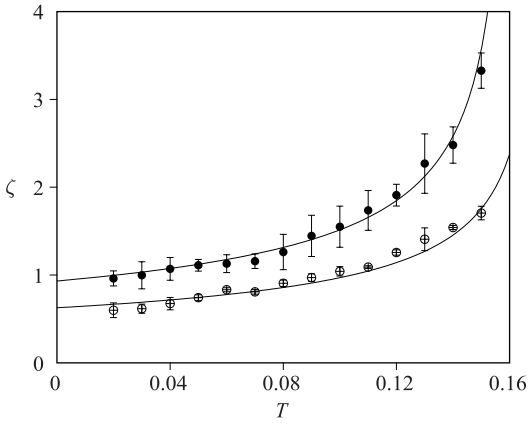

Fig. 5 Mean interface width ζ as a function of temperature T for $n = 5$ (*solid circles*) and $n = 8$ (*open circles*) at $t = 10^5$ iterations. Fixed parameter $\kappa = 5$. Continuous lines correspond to Eq. (8).

minimum value. This indicates that the repulsion between species due to collisions, as represented in Eq. (4), becomes maximum for $\kappa > \kappa_c$.

The effect of the temperature on the interface width can be approximated using the classical Ising model for an interface between two species [38],

$$\zeta \sim \frac{1}{(T_c - T)^{1/2}}, \tag{8}$$

where T_c is the critical temperature for interface formation.

In Fig. 5, we compare the numerical results obtained from our model with the values given by Eq. (8) for two different values of n. There is good agreement between the behavior described by Eq. (8) and the simulations. The critical temperatures calculated from the fitting of the numerical points to Eq. (8) are $T_c \approx 0.162$ for $n = 5$ and $T_c \approx 0.173$ for $n = 8$.

Another property that characterizes an interface is the interfacial tension, denoted by Γ. A simple way to estimate Γ is through the expression [38]

$$\Gamma \sim \frac{4\rho^\gamma_\infty}{3\zeta}. \tag{9}$$

Figure 6 shows the Γ values obtained from Eq. (9) as a function of temperature. The simulation points are compared with the theoretical expression for interfacial tension given by the Ising model [38],

$$\Gamma \sim \frac{(T_c - T)^{3/2}}{T}. \tag{10}$$

Note that for temperatures $T \geq 0.06$, the interfacial tension values calculated from the simulations and Eq. (9) are well fitted by the theoretical curve from Eq. (10).

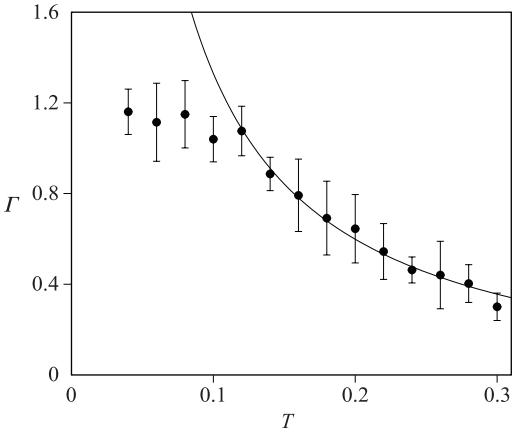

Fig. 6 Interface tension Γ as a function of temperature T at $t = 10^4$ iterations. Fixed parameter values are $\rho_0^\gamma = 5$, $\kappa = 5$. Continuous line corresponds to Eq. (10).

It is known from direct molecular dynamics simulations with two immiscible Lennard–Jones fluids [40], as well as from density functional theory [41],that the interfacial tension Γ exhibits a maximum as the temperature is varied. The maximum value of Γ occurs at a temperature at which the attractive interaction forces between particles cancel out the thermal effect. For temperatures above this point, the thermal effect is sufficiently strong to cause a decrease in the value of Γ. Our multiparticle collision binary fluid model agrees well with the behavior of Γ predicted by the Ising model for temperatures at which the thermal effect is dominant. However, in this model, the attractive interaction forces between particles are not explicit but are represented by rotation operators.

3.3 Phase separation

Next, we consider the problem of phase separation of an immiscible binary fluid in the framework of our model. The dimensions of the sides of the box are $L_x = L_y = 100$ and $L_z = 2$, and we assume that the volume has periodic boundary conditions on all three axes. We start from homogeneous initial conditions where both species are uniformly distributed in the volume of the simulation box.

Figure 7 shows four snapshots of the evolution of the system. The initial well-mixed state is displayed in Fig. 7(a). Figures 7(b)–(d) show the spontaneous formation of a segregated state at successive times, where the domains become separated by a thin interface.

Domain growth can be characterized by the time evolution of the average radius as

$$R_t \sim t^\alpha, \tag{11}$$

where R_t is the average radius of the phase domain at time t, and α is the growth exponent. We define the average radius R_t as the distance r at which the spatial correlation function $C[r,t]$ first becomes zero; that is

$$R_t = \min\{r \forall C[r,t]\} = 0. \tag{12}$$

The spatial correlation function using the discrete cells of the model can be calculated as

$$C[r,t] = \langle \Phi_t(\xi)\Phi_t(\xi')\rangle_{\xi,\xi'}, \tag{13}$$

where $r = |\boldsymbol{r}_\xi - \boldsymbol{r}_{\xi'}|$ is the distance between the center of cell ξ and the center of cell ξ', $\langle\cdots\rangle_{\xi,\xi'}$ is the spatial average over all pairs of cells ξ and ξ' separated by a distance r, and

$$\Phi_t(\xi) = \rho_t^\gamma(\xi) - \rho_t^{\gamma^*}(\xi) \tag{14}$$

is the difference between the densities of species γ and γ^* in cell ξ at time t.

Figure 8 shows a log–log plot of R_t as a function of time for a fixed temperature. The logarithm of the radius R_t increases linearly with the logarithm of time in the

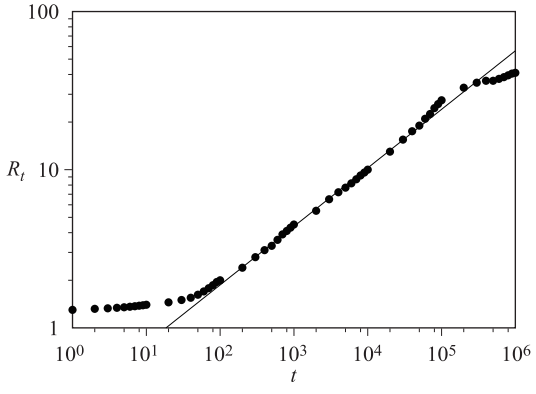

Fig. 8 Average radius of a domain phase R_t, shown as black dots, as a function of time t in log–log scale. Fixed parameter values are $L_x = L_y = 200$, $L_z = 2$, $\rho_0^\gamma = 5$, $T = 0.09$, and $\kappa = 5.0$. The continuous line corresponds to the best fitting of Eq. (11) for points in the interval $t \in [10^2, 10^5]$.

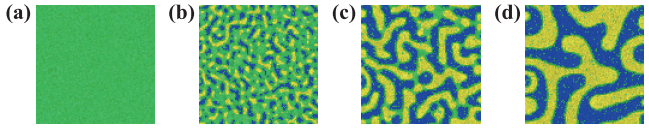

Fig. 7 Snapshots along the z axis of the patterns during the evolution of the system for fixed parameter values $L_x = L_y = 100$, $L_z = 2$, $\rho_0^\gamma = 5$, $T = 0.09$, and $\kappa = 5.0$. Particles of species A appear in yellow (*light gray*), and particles of species B are marked in blue (*black*). Green (*dark gray*) indicates the presence of particles of both species. The color intensity is proportional to the particle density. **(a)** Initial condition. **(b)** $t = 10^2$. **(c)** $t = 10^3$. **(d)** $t = 10^4$.

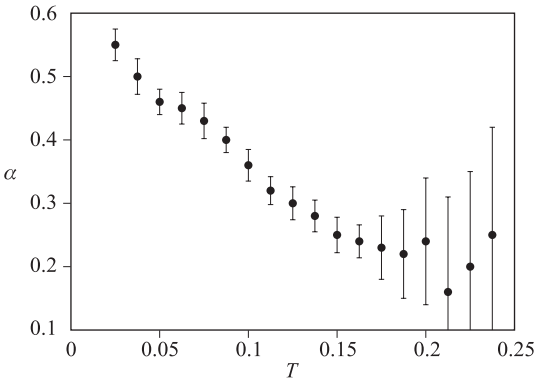

Fig. 9 Growth exponent α as a function of temperature T. Fixed parameter values are $L_x = L_y = 100$, $L_z = 2$, $\rho = 5$, and $\kappa = 5.0$. Error bars represent the standard error of the fit of Eq. (11).

interval $t \in [10^2, 10^5]$. The corresponding slope, obtained by fitting the data, yields the growth exponent $\alpha \approx 0.37$, which is close to the theoretical value $\alpha = 1/3$ for phase growth in a diffusive regime [39]. For times greater than $t = 10^5$, the domain size reaches half the size of the simulation box (that is, $R_t \approx L_x/4$), and the domain growth slows down.

Figure 9 shows the growth exponent α as a function of the temperature T calculated numerically from data in the time interval for which Eq. (11) is valid. The exponent α decays linearly with increasing temperature up to a value of $T \approx 0.2$. Above this critical temperature, the error bars in the determination of the quantity α are too large, and the interface becomes unstable because thermal mixing halts the phase separation process.

4 Binary fluid in a crowded environment

The motion of fluids in a crowded environment with obstacles is a highly interesting problem in cell biology and other contexts [42–44]. One way of modeling a fluid film in a crowded environment is by placing a set of cylindrical obstacles in the system [30]. To simulate the behavior of a binary fluid in a crowded environment using our model, we insert N_S stationary cylinders in a volume of radius σ with a height equal to the height of the simulation box L_z. The fraction of the volume occupied by the obstacles is $\phi = 2\pi N_S \sigma^2 L_z/\mathcal{V}$. We fix the radius of the cylinders at $\sigma = 2.5$ in units of cells.

As in the previous simulations, particles of one species are distributed uniformly in the right half of the simulation box, and particles of the other species are distributed on the left half of the box. We set the particle velocities using a Boltzmann distribution with temperature T and fix the densities $\rho = \rho^\gamma = \rho^{\gamma*} = 5$ and the repulsion parameter at $\kappa = 5$. We assume that when a particle of either species collides with an obstacle, its velocity is reversed, i.e., a bounce-back collision occurs.

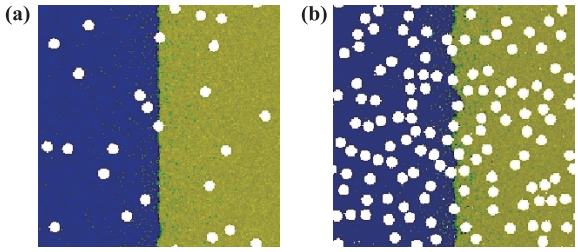

Fig. 10 Snapshots along the z axis of the system forming a stable interface at $t = 10^4$ iterations for different values of the volume fraction of obstacles ϕ. White circles indicate the cylindrical obstacles. Fixed parameters are $\rho = 5$, $\kappa = 5.0$, and $T = 0.06$. **(a)** $\phi = 0.05$. **(b)** $\phi = 0.25$.

Figure 10 shows two snapshots of the system when the interface has stabilized for different values of the volume fraction occupied by obstacles. Note that the interface lies close to obstacles and appears distorted. This effect is a consequence of the reduction in pressure that occurs when the distance between the interface curve and an obstacle is small enough to produce an imbalance of forces that removes the particles lying between the interface and the obstacle.

We also study spontaneous phase separation of an immiscible binary fluid in a crowded environment. In this case, the particles of each species are initially distributed uniformly throughout the volume of the simulation box, avoiding the space occupied by the obstacles.

Figure 11 shows snapshots of the evolution of the phase growth processes for three different values of the volume

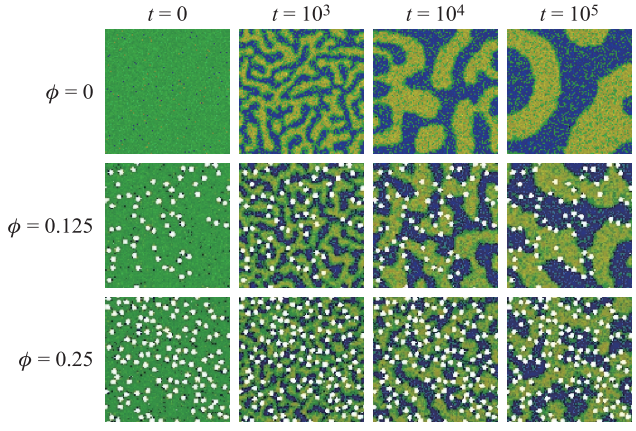

Fig. 11 Snapshots along the z axis of the evolution of the phase growth for three values of the volume fraction, $\phi = 0.0$, 0.125, and 0.25 (from top to bottom) and four times, $t = 0$, 10^3, 10^4, and 10^5 (from left to right). White circles indicate the cylindrical obstacles. Fixed parameter values are $\rho^\gamma = \rho^{\gamma*} = 5$, $\kappa = 5.0$, and $T = 0.09$.

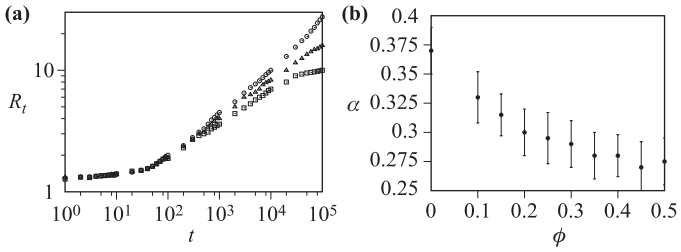

Fig. 12 **(a)** Average radius of the phase domain R_t as a function of time t in the presence of obstacles in log–log scale for $\phi = 0.0$ (*circles*), $\phi = 0.125$ (*triangles*), and $\phi = 0.25$ (*squares*). **(b)** Growth exponent α as a function of ϕ in the presence of obstacles. Fixed parameter values are $L_x = L_y = 50$, $L_z = 2$, $\rho^{\gamma} = \rho^{\gamma *} = 5$, $T = 0.09$, and $\kappa = 5.0$. Error bars represent the standard error of the fit of Eq. (11).

fraction of obstacles ϕ. As expected, phase growth from a homogeneous state is affected by the presence of obstacles. At first glance, we can see that growth becomes slower when ϕ is increased, as obstacles impede the aggregation of particles in domains. Additionally, we see that the interfaces lie along the locations of obstacles, lacking the rounded profile that they possess when the medium is free.

To investigate the effect of obstacles on the phase growth process, we calculated the time evolution of the average radius of the phase domain R_t for several values of ϕ, as shown in Fig. 12(a). For each value of ϕ, R_t can be adjusted to the expression Eq. (11) in the time interval $t \in [10^2, 10^5]$. This allows us to calculate the growth exponent α as a function of ϕ, as shown in Fig. 12(b). Increasing the density of obstacles leads to a decrease in the velocity of the phase growth process, which is represented by the exponent α.

5 Conclusions

We proposed a multiparticle collision dynamics model to investigate phase separation processes in a binary fluid. To this end, we introduced a repulsion rule between the centers of mass of particles from different species to simulate segregation in a binary fluid. We applied this model to mesoscopic systems in both free and crowded environments, where the volume was discretized into finite cells.

Because the repulsion rule depends only on the configuration of the particles inside each cell, the model maintains Galilean invariance. In addition, the multiparticle collision model with repulsion conserves the mass and energy of the system at the micro- and macro-scales, whereas momentum is conserved within homogeneous domains, but not at the interfaces.

Despite this limitation, the multiparticle-collision repulsion model yields results consistent with the known behavior of binary fluids. Properties such as the diffusion coefficient, density profile, and width of the interface calculated from simulations of the multiparticle-collision repulsion model agree very well with the theoretical values predicted by the Ising model for interfaces in a wide range of temperatures and densities. For moderate and low temperatures, the model can simulate the segregation of an immiscible binary fluid into domains, starting from mixed, homogeneous initial conditions. Moreover, the growth exponents of the phases obtained from the model are similar to the corresponding growth exponents that characterize Newtonian binary fluids.

We extended the multiparticle-collision repulsion model to simulate crowded environments. The results from the simulations are also consistent with the behavior of binary fluids in these environments.

The good performance of the multiparticle-collision repulsion model for a binary fluid suggests that it can be generalized to incorporate other phenomena, such as chemical reactions among the species, and to consider species that may diffuse at different rates. In addition, because of its low computational cost, the multiparticle-collision repulsion model can be used to simulate systems with relatively large temporal and spatial scales, i.e., to simulate systems with millions of particles for millions of iterations.

Acknowledgements This work was supported in part by project No. C-1804-12-05-B of Consejo de Desarrollo Científico, Humanístico, Tecnológico y de las Artes, Universidad de Los Andes, Mérida, Venezuela. M. G. C. is grateful to the Associates Program of the Abdus Salam International Centre for Theoretical Physics, Trieste, Italy, for visiting opportunities.

References

1. M. Müller, D. Charypar, and M. Gross, Particle-based fluid simulation for interactive applications, in: Proceedings of the 2003 ACM SIGGRAPH/Eurographics Symposium on Computer Animation, pp 154–159 (2003)
2. S. Premžoe, T. Tasdizen, J. Bigler, A. Lefohn, and R. T. Whitaker, Particle-based simulation of fluids, *Comput. Graph. Forum* 22(3), 401 (2003)
3. Z. G. Mills, W. Mao, and A. Alexeev, Mesoscale modeling: Solving complex flows in biology and biotechnology, *Trends Biotechnol.* 31(7), 426 (2013)
4. M. G. Saunders and G. A. Voth, Coarse-graining methods for computational biology, *Annu. Rev. Biophys.* 42(1), 73 (2013)
5. U. Frisch, B. Hasslacher, and Y. Pomeau, Lattice-gas automata for the Navier–Stokes equation, *Phys. Rev. Lett.* 56(14), 1505 (1986)

6. S. Succi, The Lattice Boltzmann Equation for Fluid Dynamics and Beyond, Oxford: Oxford University Press, 2001
7. G. Falcucci, S. Ubertini, and S. Succi, Lattice Boltzmann simulations of phase-separating flows at large density ratios: The case of doubly-attractive pseudo-potentials, *Soft Matter* 6(18), 4357 (2010)
8. G. Falcucci, G. Bella, G. Shiatti, S. Chibbaro, M. Sbragaglia, and S. Succi, Lattice Boltzmann models with mid-range interactions, *Commun. Comput. Phys.* 2, 1071 (2007)
9. G. Falcucci, S. Ubertini, C. Biscarini, S. D. Francesco, D. Chiappini, S. Palpacelli, A. D. Maio, and S. Succi, Lattice Boltzmann methods for multiphase flow simulations across scales, *Commun. Comput. Phys.* 9(02), 269 (2011)
10. P. J. Hoogerbrugge and J. Koelman, Simulating microscopic hydrodynamic phenomena with dissipative particle dynamics, *Europhys. Lett.* 19(3), 155 (1992)
11. R. D. Groot and P. B. Warren, Dissipative particle dynamics: Bridging the gap between atomistic and mesoscopic simulation, *J. Chem. Phys.* 107(11), 4423 (1997)
12. P. Español and M. Revenga, Smoothed dissipative particle dynamics, *Phys. Rev. E* 67(2), 026705 (2003)
13. A. Malevanets and R. Kapral, Mesoscopic model for solvent dynamics, *J. Chem. Phys.* 110(17), 8605 (1999)
14. A. Malevanets and R. Kapral, Solute molecular dynamics in a mesoscale solvent, *J. Chem. Phys.* 112(16), 7260 (2000)
15. A. Malevanets and R. Kapral, Mesoscopic multi-particle collision model for fluid ow and molecular dynamics, in: Novel Methods in Soft Matter Simulations, Eds. M Karttunen, I. Vattulainen, and A. Lukkarinen, Berlin: Springer, 2003
16. G. Gompper, T. Ihle, K. Kroll, and R. G. Winkler, Multi-particle collision dynamics: A particle-based mesoscale simulation approach to the hydrodynamics of complex fluids, advanced computer simulation approaches for soft matter sciences III, *Adv. Polym. Sci.* 221, 1 (2009)
17. J. T. Padding and A. A. Louis, Hydrodynamic and Brownian fluctuations in sedimenting suspensions, *Phys. Rev. Lett.* 93(22), 220601 (2004)
18. M. Hecht, J. Harting, M. Bier, J. Reinshagen, and H. J. Herrmann, Shear viscosity of claylike colloids in computer simulations and experiments, *Phys. Rev. E* 74(2), 021403 (2006)
19. K. Mussawisade, M. Ripoll, R. G. Winkler, and G. Gompper, Dynamics of polymers in a particle-based mesoscopic solvent, *J. Chem. Phys.* 123(14), 144905 (2005)
20. M. Ripoll, R. G. Winkler, and G. Gompper, Hydrodynamic screening of star polymers in shear flow, *Eur. Phys. J. E* 23(4), 349 (2007)
21. C. Echeverria and R. Kapral, Macromolecular dynamics in crowded environments, *J. Chem. Phys.* 132(10), 104902 (2010)
22. C. Echeverria, Y. Togashi, A. S. Mikhailov, and R. Kapral, A mesoscopic model for protein enzymatic dynamics in solution, *Phys. Chem. Chem. Phys.* 13(22), 10527 (2011)
23. C. Echeverria and R. Kapral, Molecular crowding and protein enzymatic dynamics, *Phys. Chem. Chem. Phys.* 14(19), 6755 (2012)
24. C. Echeverria and R. Kapral, Diffusional correlations among multiple active sites in a single enzyme, *Phys. Chem. Chem. Phys.* 16(13), 6211 (2014)
25. H. Noguchi and G. Gompper, Dynamics of fluid vesicles in shear flow: Effect of membrane viscosity and thermal fluctuations, *Phys. Rev. E* 72(1), 011901 (2005)
26. K. Rohlf, S. Fraser, and R. Kapral, Reactive multiparticle collision dynamics, *Comput. Phys. Commun.* 179(1–3), 132 (2008)
27. K. Tucci and R. Kapral, Mesoscopic model for diffusion-influenced reaction dynamics, *J. Chem. Phys.* 120(17), 8262 (2004)
28. K. Tucci and R. Kapral, Mesoscopic multi-particle collision dynamics of reaction diffusion fronts, *J. Phys. Chem. B* 109(45), 21300 (2005)
29. C. Echevería, K. Tucci, and R. Kapral, Diffusion and reaction in crowded environments, *J. Phys.: Condens. Matter* 19(6), 065146 (2007)
30. C. Echeverria and R. Kapral, Autocatalytic reaction dynamics in systems crowded by catalytic obstacles, *Physica D* 239(11), 791 (2010)
31. Y. Hashimoto, Y. Chen, and H. Ohashi, Immiscible real-coded lattice gas, *Comput. Phys. Commun.* 129(1–3), 56 (2000)
32. Y. Inoue, Y. Chen, and H. Ohashi, A mesoscopic simulation model for immiscible multiphase fluids, *J. Comput. Phys.* 201(1), 191 (2004)
33. T. Sakai, Y. Chen, and H. Ohashi, Real-coded lattice gas model for ternary amphiphilic fluids, *Phys. Rev. E* 65(3), 031503 (2002)
34. F. Drube, Selfdiffusiophoretic Janus Colloids, Doctoral dissertation, Ludwig-Maximilians-Universität, München, 2013
35. E. Tüzel, G. Pan, T. Ihle, and D. M. Kroll, Mesoscopic model for the fluctuating hydrodynamics of binary and ternary mixtures, *Europhys. Lett.* 80(4), 40010 (2007)
36. T. Ihle and D. M. Kroll, Stochastic rotation dynamics: A Galilean-invariant mesoscopic model for fluid flow, *Phys. Rev. E* 63(2), 020201 (2001)
37. M. Laradji, S. Toxvaerd, and O. G. Mouritsen, Molecular dynamics simulation of spinodal decomposition in three-dimensional binary fluids, *Phys. Rev. Lett.* 77(11), 2253 (1996)

38. S. A. Safran, Statistical Thermodynamics of Surfaces: Interfaces and Membranes, Addison-Wesley, 1994

39. A. J. Bray, Theory of phase-ordering kinetics, *Adv. Phys.* 51, 481 (2002)

40. E. Díaz-Herrera, J. Alejandre, G. Ramirez-Santiago, and F. Forstmann, Interfacial tension behavior of binary and ternary mixtures of partially miscible Lennard-Jones fluids: A molecular dynamics simulation, *J. Chem. Phys.* 110(16), 8084 (1999)

41. S. Iatsevitch and F. Forstmann, Density profiles at liquid–vapor and liquid–liquid interfaces: An integral equation study, *J. Chem. Phys.* 107(17), 6925 (1997)

42. H. X. Zhou, G. Rivas, and A. P. Minton, Macromolecular crowding and confinement: Biochemical, biophysical, and potential physiological consequences, *Annu. Rev. Biophys.* 37(1), 375 (2008)

43. A. S. Verkman, Solute and macromolecule diffusion in cellular aqueous compartments, *Trends Biochem. Sci.* 27(1), 27 (2002)

44. L. Stagg, S. Q. Zhang, M. S. Cheung, and P. Wittung-Stafshede, Molecular crowding enhances native structure and stability of a/b protein flavodoxin, *Proc. Natl. Acad. Sci. USA* 104(48), 18976 (2007)